Environmental Science & Technology

pubs.acs.org/est

Article

Integrating Thermal Analysis and Reaction Modeling for Rational Design of Pyrolytic Processes to Remediate Soils Contaminated with Heavy Crude Oil

Ye Gao, Priscilla Dias Da Silva, Pedro J. J. Alvarez, and Kyriacos Zygourakis*

Cite This: *Environ. Sci. Technol.* 2021, 55, 11987−11996

Read Online

ACCESS | Metrics & More | Article Recommendations | Supporting Information

ABSTRACT: We developed a novel methodology that combines thermo-analytical measurements and mathematical methods to inform the reliable pyrolytic treatment of specific soil/contaminant systems. Our approach improves upon current "black-box" design methods that may overestimate the required treatment intensity and hinder cost efficacy. We used thermogravimetry and evolved gas analysis to characterize the complex network of soil mineral transformations, contaminant desorption, and pyrolytic reactions occurring when contaminated soils are heated in an anoxic atmosphere. The kinetics of these reactions were quantified using a distributed activation energy (DAE) approach with six pseudo-components and used in a mathematical model for continuous-flow reactors to predict the removal of hydrocarbon contaminants without other fitting parameters. This model was tested with pilot-scale data from pyrolytic treatment of soils contaminated with crude oil and found to be a good predictor of the total petroleum hydrocarbon (TPH) removal for temperatures between 370 and 470 °C and residence times from 15 to 60 min. The light hydrocarbon fraction desorbed quickly, and over 99.7% removal was achieved at 420 °C and 15 min residence time. However, 95% removal of the heavy hydrocarbon fraction, which is a good proxy for polyaromatic hydrocarbons (PAHs), required 470 °C with 15 min residence time. This model can be employed to select operating conditions (e.g., reactor size, treatment time, and temperature) to reliably achieve remediation objectives for specific hydrocarbon/soil mixtures without inflating energy requirements, which would lower operating costs and decrease the process carbon footprint on a system-specific basis.

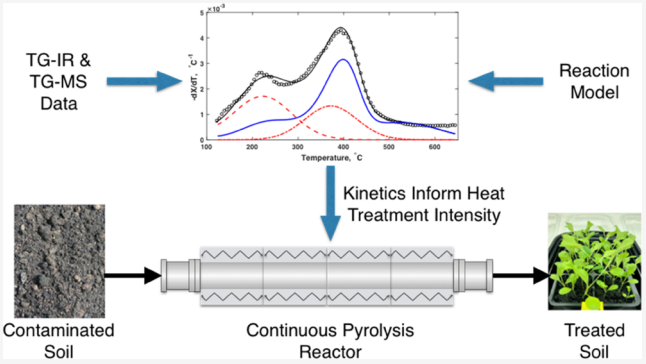

KEYWORDS: *contaminated soil, heavy hydrocarbons, thermal remediation, pyrolysis, thermogravimetry, chemical reaction kinetics, reactor modeling*

INTRODUCTION

There is a pressing need for reliable, broadly applicable, and sustainable remediation of soils impacted by polyaromatic hydrocarbons (PAHs) and other persistent hydrophobic hazardous pollutants. Whereas numerous site remediation approaches have been developed, many of these technologies are marginally cost effective or unreliable.[1−5] For example, bioremediation (including landfarming) is relatively slow, often difficult to accomplish,[6−11] and has the potential to generate more toxic PAH byproducts.[12]

We recently demonstrated that pyrolytic treatment of contaminated soils under carefully selected operating conditions can rapidly and reliably remove heavy hydrocarbons (including PAHs)[13,14] and eliminate toxicity to human lung cells[14] while preserving the fertility of the soil to facilitate ecosystem restoration and regreening efforts.[13,14] The advantages of pyrolytic treatment over other thermal treatment methods like incineration include significantly lower energy requirements and preservation of soil fertility, due to retention of some organic carbon and water holding capacity.[13−15] More recent studies confirmed the advantages of pyrolytic treatment by demonstrating high hydrocarbon removal efficiencies.[16,17] Like other thermal treatment processes, pyrolytic treatment could emit toxic volatile compounds. However, such emissions are mitigated by off-gas collection, reuse, and incineration or adsorption units.[18,19]

Thermogravimetry and evolved gas analysis (EGA) with online mass spectrometry and infrared analysis revealed that pyrolytic treatment of soils contaminated with petroleum crudes proceeds in two stages.[15] The more volatile contaminants

Received: June 4, 2021
Revised: August 13, 2021
Accepted: August 13, 2021
Published: August 25, 2021

desorb as the soil is heated to 350 °C. When temperatures rise above 350 °C, however, heavier hydrocarbons (including PAHs) undergo pyrolytic reactions that release hydrogen and C_1-C_4 hydrocarbons as they form a carbonaceous material (coke) that is nontoxic and refractory to further chemical reactions.[20−25] Coke formation is usually triggered by heterogeneous catalysis and proceeds via a cascade of reactions that include radical formation via hydrogen abstraction or C−C bond breaking, and propagation via β-scission or cyclization.[26−28] PAHs play a big role in this process via the formation of aryl radicals.[28] The final product is a 5−10 μm thick coke layer with a polynuclear aromatic character that coats the surface of soil particles, as we demonstrated with X-ray photoelectron spectroscopy (XPS) and elemental analysis.[15]

Pyrolytically treated soils exhibit significant differences in fertility, as determined by germination and biomass production metrics.[13,14] Our previous studies also revealed potential tradeoffs between pyrolytic treatment intensity (and associated energy consumption), soil detoxification efficacy, and soil fertility restoration. For one contaminated soil, for example, treatment at 420 °C for 30 min resulted in high contaminant removal efficiencies (99.9% for total petroleum hydrocarbons (TPH) and 94.5% for PAHs) and restored fertility to clean soil levels.[14] When the same soil was treated at 470 °C for 15 or 30 min, however, its fertility was reduced to 51 and 39%, respectively, of the clean soil level, which was only marginally better than that of the contaminated soil.[14]

Since different soil/hydrocarbon mixtures may respond differently to pyrolytic treatment, the design and operation of remediation processes should be system specific. A deeper mechanistic understanding of the fundamental pyrolysis processes is necessary to select treatment conditions that achieve multiple objectives like detoxification and soil fertility restoration in addition to contaminant removal. More specifically, we need a better quantitative understanding of the interactions between (a) thermally induced changes to soil components that will affect the fertility of treated soils and (b) contaminant desorption and pyrolysis that will ultimately determine their removal rate and extent. However, the operating conditions for current thermal remediation processes are often selected using empirical approaches that do not address the complexity of the soil/contaminant systems and may exaggerate the required heat treatment intensity. This inflates energy consumption and the associated treatment cost and carbon footprint. Thus, there is a need for comprehensive testing protocols that quantify soil/contaminant interactions and integrate robust data analysis and reactor modeling to inform the selection of cost effective and more sustainable operating conditions for pyrolytic treatment.

To address this need, we present here a novel approach that combines advanced analytical measurements and mathematical methods to inform the pyrolytic treatment of specific soil/contaminant systems without relying on "black-box" methods. We first demonstrate how to use thermogravimetry and evolved gas analysis to (a) model the complex network of decomposition and pyrolysis reactions occurring when contaminated soils are heated in an anoxic atmosphere and (b) quantify the kinetics of these reactions. Using a two-step methodology, we analyze and model the thermal transformations of soil components before characterizing the desorption and pyrolysis of contaminants. We then use the full pyrolysis kinetics to develop a reactor model that can predict the conversion of key contaminants and decomposition of soil components as they are heated in a continuous pyrolysis reactor. We show how this model can be used to select reactor operating conditions that reliably achieve remediation objectives without extreme heat treatment intensities, thus enhancing the cost efficacy and decreasing the associated carbon footprint. Finally, we test this model with pilot-scale results presented earlier[14] for pyrolytic treatment of soils contaminated with crude oil.

MATERIALS AND METHODS

Contaminated Soil Samples and Pyrolysis Experiments in a Continuous Reactor. Two contaminated soils and their background (clean) soil were used for this study.[14] Both contaminated soils were pyrolytically treated in a pilot-scale rotary kiln reactor (Hazen Research, Golden, CO) at three pyrolysis temperatures (370, 420, and 470 °C) and 15, 30, and 60 min residence times.[14] Additional details about the operation of this reactor are provided in the Supporting Information section. Pyrolytically treated soils were analyzed for TPH and PAH content by the Eurofins Lancaster Labs (Lancaster, PA). The TPH concentration was determined by measuring the solvent-extractable hydrocarbons via the gas chromatography-flame ionization detector (GC-FID) according to the EPA 8015M method. The 16 U.S. EPA priority pollutant PAH compounds were analyzed by EPA Method 8270C (SW-846).

Evolved Gas Analysis (EGA) of Clean and Contaminated Soils. Thermogravimetric analysis experiments with online infrared gas analysis (TG-IR) were performed using a thermogravimetric analyzer (TGA) (Q500, TA Instruments, New Castle, DE) connected to a nondispersive infrared (NDIR) gas analyzer (LI-840A, LI-COR, Lincoln, NE). Since all of the gas exiting the TGA flows through its optical path, the online NDIR instrument allows for continuous quantitative measurement of CO_2 and H_2O concentrations in the gaseous stream exiting the thermogravimetric analyzer. For all TG-IR experiments, 50−60 mg of either clean or contaminated soils were placed on a platinum pan and treated in the TGA under high-purity nitrogen flowing at a rate of 100 mL/min. To remove the sample moisture, every run started with a drying stage in which the temperature was raised to 105 °C and held there for 30 min. When the drying stage was complete, the temperature was ramped to a final value of 650 °C at a constant heating rate of 1 °C/min. Every sequence of TG-IR experiments started with two blank runs using the same method but without any samples to flush the air from the system and stabilize the readings of the IR instrument. Data from several thermogravimetric experiments were used to compute the average weight loss of the soil and evolved gas concentrations, all of which were highly reproducible (Figure S1). Note that the relatively slow heating rate of 1 °C/min was used to minimize the temperature lag between measured and actual sample temperature and improve the accuracy of the measurements used for estimating the kinetic parameters of pyrolysis reactions.

DAE Model for Pyrolysis Kinetics. Thermal analysis experiments (TG-IR and TG-MS) were carried out to characterize the thermal transformations of soil components as well as the desorption and pyrolysis of hydrocarbon contaminants. Using this data, we grouped the numerous species of clean and contaminated soils into a small number of pseudocomponents. Each pseudocomponent consists of a large number of compounds (e.g., clays, minerals, soil organic matter, and different hydrocarbon contaminants) that pyrolyze at their own species-specific rates. To simplify the kinetic analysis, however, we assumed that each pseudocomponent reacts as a

https://doi.org/10.1021/acs.est.1c03607
Environ. Sci. Technol. 2021, 55, 11987−11996

single species but with an activation energy that is distributed according to a Gaussian probability density function.[29] This is the core assumption of the distributed activation energy (DAE) approach introduced by Vand[30] and used by others to model the pyrolysis kinetics of coal[31−34] and lignocellulosic biomass.[35−41] To estimate the kinetic parameters of all decomposition reactions, we solved an optimization problem that matched the sum of the pseudocomponent weight losses predicted by the DAE model to the experimental weight losses measured by thermogravimetry.[29] The Supporting Information section provides details of the conceptual development and the mathematical formulation of our DAE model. Note that all kinetic parameters of the pyrolysis reactions were obtained from thermogravimetric experiments with clean and contaminated soils.

RESULTS AND DISCUSSION

Kinetics of Clean Soil Pyrolysis. Since 90−95% of the mass of petroleum-contaminated soils consists of soil minerals, thermal transformations of soil components (like clay dehydration or carbonate decomposition) account for a large fraction of the weight losses observed during pyrolysis. Moreover, the temperature ranges of soil mineral transformations overlap with the temperature ranges over which desorption and pyrolysis of contaminants take place.[15,29] This overlap necessitates the use of a two-step approach to decouple the kinetics of soil transformations from those of contaminant desorption and pyrolysis.

The solid thick lines of Figure 1a,b present the thermogravimetry (TG) and differential thermogravimetry (DTG) curves describing the average weight $w(T)$ and the average weight loss rate dw/dT of the clean soil as it is heated at a constant rate in a thermogravimetric analyzer.[15,29] Data from several thermogravimetric experiments were used to compute the average weight loss of our clean soil, which was highly reproducible (Figure S1).

Background soil weight losses (Figure 1a) are primarily due to the release of water and carbon dioxide as various soil components and minerals undergo thermal transformations upon heating.[15] Water is released as vapor from the clay components of the soil, which retain substantial amounts of water between their two-dimensional silicate sheets[42−47] and are responsible for its fertility.[13,14,45] Reversible dehydration occurs at temperatures lower than 500 °C,[48−50] while irreversible dehydroxylation may lead to water release at temperatures usually higher than 500 °C through a two-step proton transfer by two hydroxyl groups.[47,51−54] Finally, carbon dioxide is released as the small amounts of organic matter (SOM) present in this soil pyrolyze in the nitrogen atmosphere of the TGA.[15,55]

The observed decomposition rate (Figure 1b) is a convolution or sum of multiple water and carbon dioxide peaks, each one of them coming from different fractions of soil. This overall soil decomposition rate can be deconvolved to determine the kinetics of soil pyrolysis using the DAE methodology.[29] First, we use EGA data from TG-IR and TG-MS experiments to group this soil into four pseudocomponents, each of which decomposes to release either water or carbon dioxide. Three pseudocomponents (denoted by A_1, A_2, and A_3) release water and model the dehydration and dehydroxylation of soil minerals (clays). Since the CO_2 release pattern had only one broad peak spanning almost the entire temperature range tested, one pseudocomponent (A_4) is sufficient to model weight losses associated with the release of carbon dioxide from SOM pyrolysis. These four parallel decomposition reactions follow

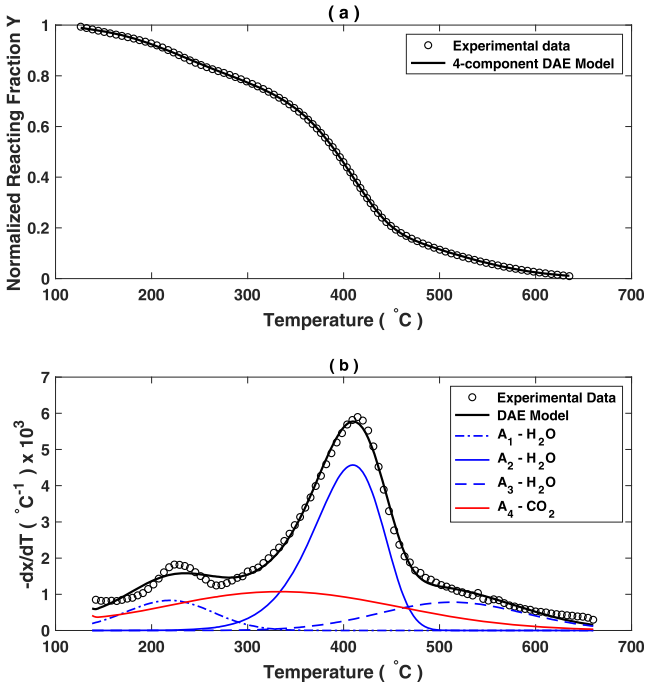

Figure 1. DAE model with four pseudocomponents accurately matches the measured weight losses and the total decomposition rate of the background (clean) soil. Panel (a): Comparison of total unreacted fraction computed by the DAE model (solid line) and measured by thermogravimetry (open symbols). Thermogravimetric data were obtained from the average of the three TGA runs. Root-mean-square error (RMSE) = 0.0019. Panel (b): Comparison of reaction rates computed by the DAE model (black solid line) and measured experimentally (open symbols). The total DAE model reaction rate is the sum of the rates of three pseudocomponents A_1−A_3 (blue lines) modeling water release and a fourth pseudocomponent A_4 (red line) modeling weight losses due to carbon dioxide release.

first-order kinetics and have activation energies distributed according to a Gaussian probability density function.[29] The DAE optimization problem was then solved to estimate the relative weight fractions of the four pseudocomponents and the kinetic parameters of their decomposition reactions: the pre-exponential factors, as well as the mean and standard deviation of the Gaussian distributions of their activation energies (Table 1).

Figure 1b shows the decomposition rates of the four pseudocomponents as Gaussian distributions (blue and red lines) whose convolution (sum) yields the overall decomposition rate of clean soil. The DAE predictions agree very well with the experimental soil decomposition rate (open circles) measured via thermogravimetry. The total weight loss (solid line of Figure 1a) predicted by the DAE model is also in excellent agreement with the thermogravimetric data (open circles in Figure 1a).

The results of Figure 1 and Table 1 are in good agreement with literature studies on water release from clays. For example, the estimated activation energies of Table 1 are well within the range of values reported in the literature,[51,56,57] a strong indication that the first two water-releasing pseudocomponents (A_1 and A_2) correspond to clay dehydration processes. Irreversible dehydroxylation is the likely thermal process represented by the A_3-H_2O pseudocomponent.

To investigate how run-to-run variability may affect the kinetics, we also estimated the kinetic parameters by (a) fitting

https://doi.org/10.1021/acs.est.1c03607
Environ. Sci. Technol. 2021, 55, 11987−11996

Table 1. Kinetic Parameters of Six-Component DAE Models for Contaminated Soils with 3 and 5% Crude Oil

Soil	Pseudocomponent	$\log_{10} k_0$ (min)	E_0 (kJ/mol)	σ (kJ/mol)	c_j	RMSE
Contaminated soil with 3% oil	A_1-H_2O	6.1	70	5.8	0.06	0.0025
	A_2-H_2O	6.8	109	2.2	0.26	
	A_3-H_2O	8.8	165	13	0.08	
	A_4-CO_2	11	158	30	0.17	
	A_5-LH	5.8	69	6.8	0.24	
	A_6-HH	12.7	168	11.5	0.19	
Contaminated soil with 5% oil	A_1-H_2O	6.1	70	5.8	0.06	0.0016
	A_2-H_2O	6.8	109	2.2	0.24	
	A_3-H_2O	8.8	165	13	0.07	
	A_4-CO_2	11	158	30	0.13	
	A_5-LH	5.8	69	6.8	0.30	
	A_6-HH	12.7	170	10.7	0.20	

thermogravimetry data from three TGA runs and (b) fitting the averaged data from these runs. The parameters computed from individual runs were within 2−5% of the values computed from the averaged data.

While a DAE model with four pseudocomponents was accurate enough for the soil considered here, additional pseudocomponents may have to be considered if the soil contains larger amounts of SOM, or if it contains carbonate minerals that decompose when heated to release significant amounts of carbon dioxide.[15]

Contaminated Soil Pyrolysis Kinetics Need Two More Pseudocomponents. Figure 2a presents the decomposition rates (or weight loss rates) for the two contaminated soils with 3 and 5% oil and compares them to the decomposition rate of the clean soil. Weight losses due to hydrocarbon devolatilization and pyrolysis superimpose two additional peaks on the multipeak decomposition rate of the clean soil shown in Figure 1. These hydrocarbon peaks appear in the temperature ranges established in our earlier work,[15] namely, 100−300 °C for desorption of light hydrocarbons and 350−450 °C for pyrolysis of heavier hydrocarbons. The height of these peaks is proportional to the crude oil content of the two contaminated soils.

The full pyrolysis kinetics of contaminated soils can therefore be determined using a DAE model with six pseudocomponents and solving an optimization problem to match DAE predictions to thermogravimetric experimental data. The first four pseudocomponents are the same used to describe soil mineral transformations that lead to the release of water and carbon dioxide during pyrolytic treatment of clean soil. A fifth pseudocomponent (A_5 or LH) models the desorption of light hydrocarbons from 100 to 350 °C, while the sixth pseudocomponent (A_6 or HH) represents heavier hydrocarbons that pyrolyze between 350 and 450 °C. Our analysis assumes that the addition of hydrocarbon contaminants does not alter the overall thermal behavior of the soil, an assumption that is supported by the relatively small amounts of added hydrocarbons (3 and 5% by weight).

The six-component DAE model fit very well the experimental weight vs temperature data for the contaminated soil with 3% crude oil (Figure 2b). Also, the convolution of the weight loss rates for the six pseudocomponents provided very good approximations to the overall weight loss rate of the 3% contaminated soil (Figure 2c). Table 1 provides the kinetic parameters estimated for both contaminated soils. Note that the mass fraction of the heavy hydrocarbon fraction (A_6-HH) for the contaminated soil with 5% crude oil is barely higher than that of the soil contaminated with 3% oil (0.20 vs 0.19) and, thus, most of the elevated weight loss of the 5% soil (Figure 2) comes from the light hydrocarbon fraction (A_5-LH).

The hydrocarbon devolatilization and pyrolysis patterns of Figure 2b are consistent with those reported for Atabasca sand bitumen that was separated into its maltene and asphaltene fractions and pyrolyzed in a TGA with 1 °C/min heating rate.[58] Perhaps one important difference is a slight shift of the conversion rate for our A_6-HH heavy hydrocarbon fraction toward lower temperatures, suggesting that soil minerals, like clays, may catalyze some pyrolytic reactions and facilitate coke deposition.[59,60] Another possible explanation is that, in our case, hydrocarbons are dispersed as a layer coating the soil particles. Mass transfer in films of heavy hydrocarbons can significantly affect the pyrolysis kinetics and the rate of coke formation.[61]

Development and Testing of a Reactor Model to Predict Contaminant Conversions. The pyrolysis kinetics obtained in the previous section was used to develop a reactor model that can predict the removal of contaminants and the conversion of any other pseudocomponents as they are heated in a continuous pyrolysis reactor. To demonstrate the predictive capability of reactor models based on first principles, we considered the pilot-scale kiln reactor used in our earlier study[14] to pyrolyze the two soils contaminated with 3 and 5% crude oil. The temperature in the pyrolysis section of the reactor (Figure S2) was kept within ±5 °C from its setpoint for most of the experiments considered here. Additional details are provided in the Supporting Information section.

As contaminated soil was fed at a constant rate in the reactor and tumbles through it, the six pseudocomponents decomposed in parallel to release gaseous products (water, carbon dioxide, volatile hydrocarbons, or hydrogen) that are swept by a constant stream of nitrogen. Using the decomposition kinetics obtained via thermogravimetry, we developed a finite-stage or mixing-cell model to describe the steady-state operation of our pyrolysis reactor. The use of a mixing-cell model was dictated by the implicit form in which decomposition rates are expressed with the integral expressions of eq S6. It is well known, however, that mixing-cell models can accurately model the operation of tubular flow reactors as long as a sufficiently large number of mixing cells (or finite stages) is used.[62−65]

The pyrolysis reactor was divided into N compartments of volume $\Delta V = A_c \Delta z$, where A_c is the cross-sectional area of the reactor (Figure 3). Since the overall weight loss is relatively small (5.64 and 7.32 wt %, respectively, for contaminated soils with 3 and 5% crude oil) and since a significant fraction of the hydrocarbons remains in the soil as char, we assumed that the volumetric flow rate was constant.

https://doi.org/10.1021/acs.est.1c03607
Environ. Sci. Technol. 2021, 55, 11987−11996

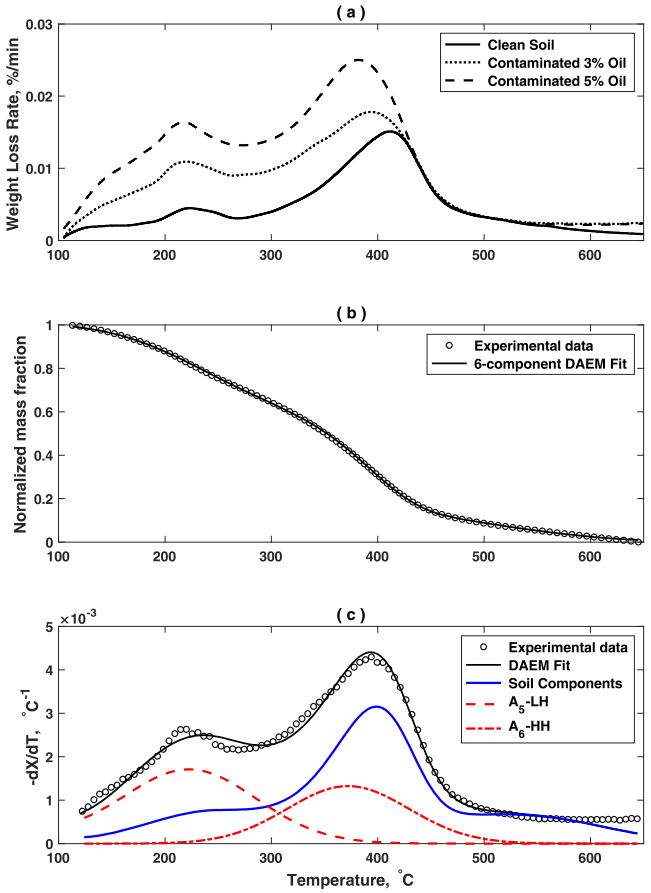

Figure 2. Addition of two pseudocomponents describing the desorption and pyrolysis of hydrocarbons allows the DAE model to accurately match the experimental decomposition rates of the contaminated soil with 3% crude oil. Panel (a): weight loss or decomposition rates for the clean soil (solid line), the contaminated soil with 3 wt % oil (dotted line), and the contaminated soil with 5 wt % oil. All lines are obtained from the averages of three TGA experiments. Panel (b): total unreacted fraction computed by the six-component DAE model for the 3% contaminated soil (solid line) and measured by thermogravimetry (symbols). The thermogravimetric data were the average of three TGA runs. RMSE = 0.0025. Panel (c): the decomposition rate computed by the six-component DAE model for the 3% contaminated soil (solid black line) matches well with the rate measured via thermogravimetry (symbols). The DAE model rate is the sum of the decomposition rates for the four soil pseudocomponents (blue solid line), the rate of the light hydrocarbon (A_5 or LH) fraction (red dashed line), and the rate of the heavy hydrocarbon (A_6 or HH) fraction (red dashed-dotted line).

Let now $\rho_i^j(t)$ be the density of the solid ith pseudocomponents in the jth compartment and R_i^j be the rate (in kg/s) at which this pseudocomponent decomposes. Then, the transient mass balances for all six pseudocomponents in this compartment yield

$$\frac{\partial}{\partial t}(\rho_i^j A_c \Delta z) = Q_s(\rho_i^{j-1} - \rho_i^j) - R_i^j,$$
$$i = 1, 2, \ldots, 6; \; j = 1, 2, \ldots, N \tag{1}$$

where Q_s is the total volumetric flow rate of the contaminated soil.

The control system of our reactor kept the pyrolysis temperature within ±5 °C of the setpoint temperature for most experiments. Moreover, samples of treated soil were collected during periods when this constraint was satisfied. Thus, we can assume that the reactor operates isothermally and at steady state, which simplifies eq 1 to

$$0 = Q_s(\rho_i^{j-1} - \rho_i^j) + R_i^j$$
$$\text{or } \rho_i^j = \rho_i^{j-1} + \frac{R_i^j}{Q_s}, \quad i = 1, 2, \ldots, 6; \; j = 1, 2, \ldots, N \tag{2}$$

After the soil has been exposed to the pyrolysis temperature for a time t, the conversion of each pseudocomponent is defined as

$$x_i(t) = \frac{m_i^0 - m_i(t)}{m_i^0} = 1 - \frac{m_i(t)}{m_i^0} \tag{3}$$

where m_i^0 is the mass of the ith pseudocomponent entering the first compartment and $m_i(t)$ is the mass that remains unreacted. Using the definition of the reaction rate, we finally obtain

$$R_i^j = \frac{\mathrm{d}m_i(t)}{\mathrm{d}t} = -m_i^0 \frac{\mathrm{d}x_i(t)}{\mathrm{d}t} \tag{4}$$

Note that when the contaminated soil leaves the jth compartment of the isothermal reactor model, it has been exposed to the pyrolysis temperature T for a total time equal to

$$t_j = \frac{j \cdot \Delta z}{v} \tag{5}$$

where v is the constant axial velocity of the soil. Equation 2 through eq 4 now yield

$$\rho_i^j = \rho_i^{j-1} - \frac{m_i^0}{Q_s}\frac{\mathrm{d}x_i}{\mathrm{d}t} \quad i = 1, 2, \ldots, 6; \; j = 1, 2, \ldots, N$$

The time derivative of conversion can now be obtained from eq S6 to yield

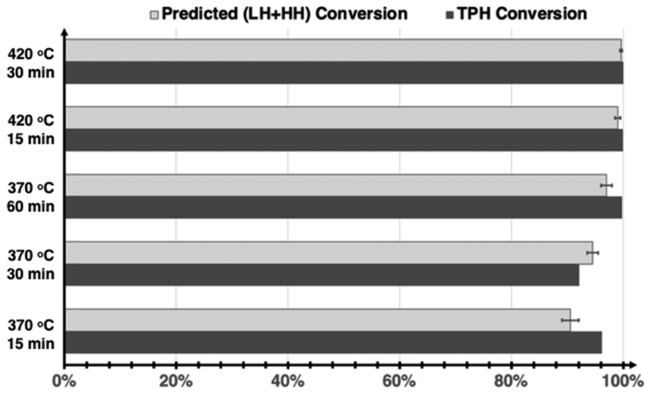

Figure 3. Model predictions using eq 8 (light gray bars) are in good agreement with the experimentally measured TPH removal percentages (dark gray bars). Differences between model predictions and measured TPH removal range from −2.4 to 5.5% for the soils treated at 370 °C and are less than 0.9% for the soils treated at 420 °C. Actual differences may be even smaller if we consider possible deviations from reactor isothermality. Note that one TPH measurement per sample was performed. The bars for the model predictions indicate the range of conversions obtained by varying the isothermal reactor temperature by ±5 °C.

https://doi.org/10.1021/acs.est.1c03607
Environ. Sci. Technol. 2021, 55, 11987−11996

$$\rho_i^j = \rho_i^{j-1} - \frac{m_i^0}{Q_s}\left[\int_0^\infty k_{i0}\exp\left(-\frac{E_i}{RT} - \int_0^{t_j} k_{i0}\, e^{-E_i/RT}\mathrm{d}\tau\right) f_i(E)\mathrm{d}E\right], \quad i = 1, 2, \ldots, 6 \tag{6}$$

where $j = 1, 2, \ldots, N$, $k_{i,0}$ are the pre-exponential reaction rate factors and $f_i(E)$ are the probability density functions for the activation energies of the pseudocomponents $i = 1, 2, \ldots, 6$.

The total density ρ_{tot}^j of the six reacting pseudocomponents can similarly be obtained as

$$\rho_{tot}^j = \rho_{tot}^{j-1} - \frac{1}{Q_s}\left[\sum_{i=1}^{6} c_i m_i^0 \int_0^\infty k_{i0} \exp\left(-\frac{E_i}{RT} - \int_0^{t_j} k_{i0}\, e^{-E_i/RT}\mathrm{d}\tau\right) f_i(E)\mathrm{d}E\right], \quad i = 1, 2, \ldots, 6 \tag{7}$$

for all $j = 1, 2, \ldots, N$. Equation 6 can now be used to compute the densities or conversions of the pseudocomponents along the length of the isothermal reactor. Once the pyrolysis temperature, the volumetric flow rate of contaminated soil, and the reactor dimensions have been specified, eq 6 provides the conversions of the six pseudocomponents at every axial position inside the isothermal reactor. All of the other model parameters needed for these computations (i.e., the reaction rate coefficients k_{i0}, the mean $E_{i,0}$ and variance σ_i^2 of the activation energy distributions, and mass fractions c_i of the six pseudocomponents) have been previously obtained by the DAE model (Table 1).

We conducted a systematic study to determine the value of compartments that will give us accurate predictions of conversions for each set of operating conditions and soil type. As expected, the total and axial conversions converge for all conditions. However, the number of compartments required to achieve convergence as $N \to \infty$ varies with the kinetic parameters. When the 3% contaminated soil is treated at 470 °C with 30 min residence time, for example, the overall (exit) conversion of pseudocomponent A_2-H_2O converges with fewer than 100 compartments, while A_3-H_2O requires about 5,000 to converge. The exit conversions of the hydrocarbon-related pseudocomponents (A_5-LH, A_6-HH) also converge for N between 1000 and 5000. To ensure accuracy for all components, typical runs use 5000 compartments and require around 15 min of CPU time on a personal computer with a 2.50 GHz Intel Core i7 processor.

Our Reactor Model Accurately Predicts Contaminant Conversions. For all pyrolysis experiments, hydrocarbon conversions were obtained by measuring the total petroleum hydrocarbons (TPH) of the treated soil exiting the reactor. TPH quantifies the total amount of volatile and extractable hydrocarbons in the C_6–C_{35} range remaining in the treated soil, as determined with various methods that involve solvent extraction and chromatographic analysis.[66] Since TPH content is a universal standard for regulatory compliance, we tested the ability of our model to predict contaminant removal levels that are comparable to the measured TPH values for the same pyrolysis conditions. The metric used was the weighted average of the conversion of the two hydrocarbon fractions at the reactor exit

$$HC_{tot} = c_5 \cdot x_5(\tau) + c_6 \cdot x_6(\tau) \tag{8}$$

where τ is the residence time in the isothermal reactor, c_5 and c_6 are the mass fractions of LH and HH hydrocarbon fractions in the contaminated soils, and $x_5(\tau)$ and $x_6(\tau)$ are the LH and HH conversions at the reactor exit.

The experimental measurements showed complete TPH removal for all residence times when the pyrolysis temperature was 470 °C. Close agreement was observed between the measured TPH removal level and the hydrocarbon conversions predicted by eq 8 when the 3% contaminated soil was pyrolytically treated at 420 °C (Figure 3). The agreement was not as good for treatment at 370 °C. However, the fact that TPH removal efficiency for 370 °C did not increase monotonically with increasing residence time (as dictated by chemical reaction dynamics and predicted by the model) reflects large sample-to-sample variability for these measurements. Note also that the residual TPH measured value strongly depends on the solubility of the remaining hydrocarbons in the solvent used for extraction and does not correspond directly to the remaining amount of the LH and HH fractions used by our reactor model.[67] Despite these limitations, the predicted conversion from eq 8 (using independently obtained rather than fitting parameters) was a good predictor for the widely used TPH metric (Figure 3), particularly since pilot-scale and commercial reactors may deviate from an isothermal operation.

Pyrolytic treatment of the 5% contaminated soil also achieved very high levels of TPH removal at all temperatures. After 30 min at 370 °C, 97.9% TPH removal was observed for the 5% contaminated soil, which was higher than the removal level measured for the 3% contaminated oil at the same conditions. Almost complete (99.8% or higher) removal was achieved after treatment at 420 and 470 °C. The hydrocarbon conversions predicted by the model and eq 8 were very similar to those reported in Figure 3 for the 3% contaminated soil. This is expected because the two contaminated soils have very similar weight fractions of the heavy hydrocarbon pseudocomponent (Table 1) and light hydrocarbon fractions require much lower temperatures for effective removal (Figure 5).

These results also suggest that TPH and hydrocarbon conversions exhibit a stronger dependence on pyrolysis temperature than on residence time. While the complexity of our model prevents us from coming up with an explicit relation of conversion as a function of temperature T and residence time τ, the simple case of an isothermal plug flow reactor (PFR) can provide a valuable insight on the relative importance of these operating parameters. When a single reaction with first-order kinetics takes place in an isothermal PFR, the overall conversion $\chi(T, \tau)$ of a reactant is given by[68]

$$\chi = 1 - \exp(-k_0\, e^{E/RT}\cdot\tau) \tag{9}$$

where k_0 and E are the pre-exponential rate constant and the activation energy of the reaction, respectively, while R is the ideal gas constant. We can then use eq 9 as a rule-of-thumb to estimate the relative effect of pyrolysis temperature and residence time on contaminant conversion. For example, the least reacting contaminant (HH hydrocarbon fraction) will exponentially approach full conversion with increasing values of the dimensionless heat treatment intensity metric $I(T, \tau)$ defined[69,70] as

$$I(T, \tau) = k_{0,6}\exp\left(-\frac{E_{0,6}}{RT}\right)\cdot\tau \tag{10}$$

https://doi.org/10.1021/acs.est.1c03607
Environ. Sci. Technol. 2021, 55, 11987−11996

where $k_{0,6}$ and $E_{0,6}$ are the pre-exponential reaction rate constant and the mean activation energy of the HH fraction. Note that for continuous reactors, the residence time τ is defined as the ratio of the reactor volume over the volumetric flow rate of the contaminated soil ($\tau = V/Q$).

The remaining concentrations of the 16 priority PAH pollutants were measured for four of the treated soils. Pyrolytic treatment was very effective in removing PAHs from these contaminated soils as shown in Table 2. The model predicted high conversions of the heavy hydrocarbon HH fraction (Table 2) and is comparable to the experimental PAH measurements, which infers that HH conversion is a good proxy for estimating PAH removal levels at different operating conditions.

Table 2. Measured PAH and Model Predicted HH Conversions

Contaminated soil	Temperature (°C)	Residence time (min)	Measured PAH conversion (%)	Model predicted HH conversion (%)
3% oil	420	15	94.5	91 ± 2
3% oil	470	30	98.7	>99.9
5% oil	420	30	99.5	93 ± 1.5
5% oil	470	15	99.6	>99.9

Reactor Model Can Inform the Choice of Optimal Operating Conditions. While eq 9 provides general trends for the effect of pyrolysis temperature and residence time on contaminant removal, the full reactor model can identify the regions of operating parameters that will achieve the desired contaminant conversion. Figure 4 plots the average contaminant conversions from eq 8 vs the pyrolysis temperature for six different residence times. The conversion curves show the expected exponential-type approach to full conversion as the pyrolysis temperature increases, while the differential effect of increasing residence time from 10 to 60 min diminishes. The simulation data show that 90% contaminant conversion can be achieved at 390 °C with a residence time of 60 min. The same level of conversion can be achieved at 395 °C with 50 min residence time, with 40 min at 400 °C or with 20 min residence time at 415 °C. To achieve 95% conversion, we need to treat the contaminated soil for 60 min at 415 °C at 60 min and 50 min at 422 °C, while we need to carry the pyrolysis at temperatures greater than 425 °C if you want a residence time of 40 min or shorter.

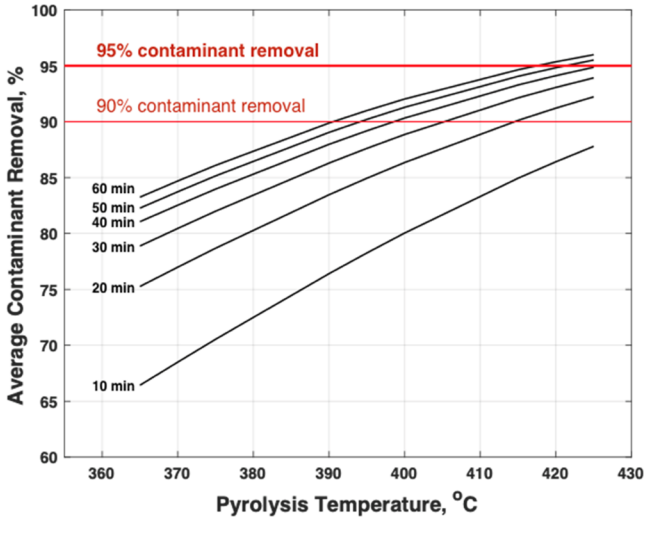

Figure 4. Reactor model can identify combinations of pyrolysis temperatures and residence times that achieve the required contaminant removal efficiency. Solid black lines present the average contaminant conversion vs pyrolysis temperature when the contaminated soil with 3% crude oil was treated for the indicated residence time. All kinetic constants are obtained from Table 1.

Reliable and predictive reactor models allow a design engineer to quickly determine a set of candidate (T, τ) pairs that will give the contaminant removal level required for regulatory compliance. How these choices affect the overall energy requirements or the economics of the process depends on several additional parameters that can only be explored with a process model that includes, in addition to the pyrolysis reactor, all of the equipment used for the transportation and comminution of the contaminated soil, the feeding of the reactor, the type of heating fuel used, the energy efficiency of the reactor, the filter used to remove the fines from the exhaust gas, etc. Yet, a good reactor model is an essential part of this process. In many cases, the minimum pyrolysis temperature yielding the desired conversion turns out to be a "good candidate" for minimizing energy use, primarily because of the large amount of energy required to raise the temperature of the soil to the pyrolysis temperature and the relatively small energy requirements of decomposition reactions.[4]

The reactor model can also provide conversion profiles of all of the pseudocomponents along the entire length of the reactor so that we can quickly explore the effects of alternative sets of parameters on reactor performance; Figure 5 shows the conversions of light hydrocarbon (LH) and heavy hydrocarbon (HH) fractions achieved for three different temperatures and a 15 min residence time in the pilot-scale reactor[14] presented in the previous sections. As expected, the LH hydrocarbon fraction desorbs very quickly and more than 95% conversion is achieved in the first half of the reactor at either 420 or 470 °C. A 95% conversion of the HH fraction, however, can be achieved in the first 75% of the reactor but only at 470 °C. Alternatively, we can use a pyrolysis temperature between 420 and 470 °C and the full length of the reactor, or set the pyrolysis temperature at 420 °C and increase the residence time. These and many more alternatives can be easily explored by multiple runs of the reactor model. In general, lower energy costs can be achieved by lowering the pyrolysis temperature, but the time required to treat a site (and all its associated costs) will increase if we increase the reactor residence time or, equivalently, decrease the solid feed rate to the reactor.

Workflow for Selecting Pyrolytic Treatment Conditions for Specific Soil/Contaminant Mixtures. By integrating thermal analysis methods and reactor modeling, the novel framework presented here outlines a systematic workflow for designing pyrolytic remediation processes considering multiple objectives, such as energy requirements and soil fertility recovery in addition to soil detoxification. This workflow, which improves upon current "black-box" approaches, has the following steps:

1. A sequence of thermal analysis tests (TG-IR, TG-MS) that (a) identify the temperatures where key soil mineral and contaminant transformations occur and (b) quantify the products of these transformations.

https://doi.org/10.1021/acs.est.1c03607
Environ. Sci. Technol. 2021, 55, 11987−11996

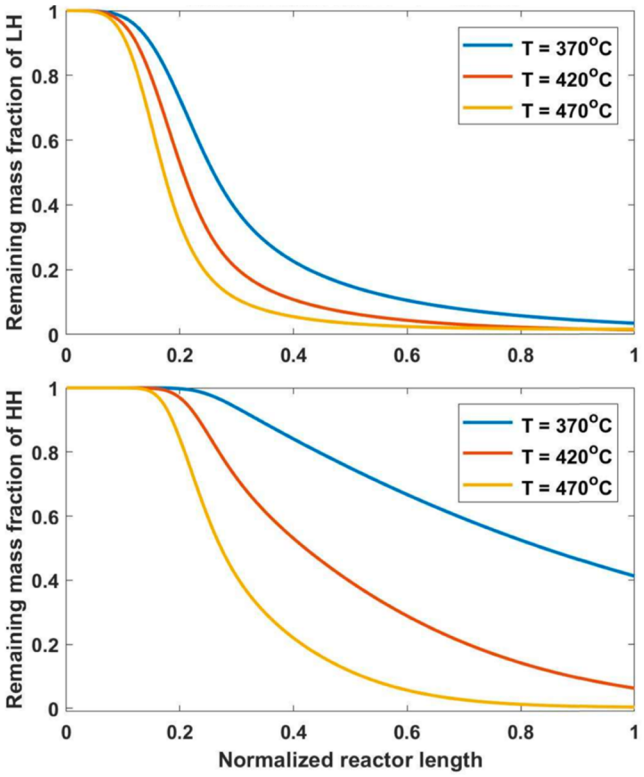

Figure 5. Predicted mass fractions of the two hydrocarbon pseudocomponents as a function of the normalized axial position (z/L) for three different pyrolysis temperatures and a solid residence time of 15 min. Contaminated soil with 3% oil was used for these simulations and the kinetic parameters are given in Table 1.

2. A distributed activation energy (DAE) methodology for deconvolving the multipeak decomposition patterns of contaminated soils to obtain the full pyrolysis kinetics.

3. A reactor model that can identify the operating conditions (pyrolysis temperature, residence time) that achieve the required contaminant conversion while avoiding high energy use or irreversible loss of soil fertility.

Since the reactor is the critical component of pyrolytic remediation systems, our novel framework represents a useful tool for remediation professionals to select appropriate cost-effective treatment conditions that are conducive to rapid, efficient, and more sustainable soil remediation, including technological decarbonization through lower energy requirements.

■ ASSOCIATED CONTENT

Supporting Information

The Supporting Information is available free of charge at https://pubs.acs.org/doi/10.1021/acs.est.1c03607.

Decomposition kinetics of complex multicomponent systems, the assumptions and key equations of the DAE method, a plot demonstrating the excellent repeatability of TG-IR experiments used to guide the selection of pseudocomponents for the clean soil, and additional details for the operation of the rotary kiln pyrolysis reactor used to treat the two contaminated soils (PDF)

■ AUTHOR INFORMATION

Corresponding Author

Kyriacos Zygourakis − *Department of Chemical and Biomolecular Engineering, Rice University, Houston, Texas 77005, United States;* orcid.org/0000-0002-1044-1139; Email: kyzy@rice.edu

Authors

Ye Gao − *Department of Chemical and Biomolecular Engineering, Rice University, Houston, Texas 77005, United States*

Priscilla Dias Da Silva − *Department of Chemical and Biomolecular Engineering, Rice University, Houston, Texas 77005, United States*

Pedro J. J. Alvarez − *Department of Chemical and Biomolecular Engineering and Department of Civil and Environmental Engineering, Rice University, Houston, Texas 77005, United States;* orcid.org/0000-0002-6725-7199

Complete contact information is available at: https://pubs.acs.org/10.1021/acs.est.1c03607

Notes

The authors declare no competing financial interest.

■ ACKNOWLEDGMENTS

Research reported in this publication was supported by the National Institute of Environmental Health Sciences of the National Institutes of Health under Award Number P42ES027725. The content is solely the responsibility of the authors and does not necessarily represent the official views of the National Institutes of Health.

■ REFERENCES

(1) Hinchee, R. E.; Smith; Lawrence, A. *In Situ Thermal Technologies for Site Remediation*; CRC Press, 1992.

(2) Stegemeier, G. L.; Vinegar, H. J. *Thermal Conduction Heating for In Situ Thermal Desorption of Soils. In Hazardous and Radioactive Waste Treatment Technologies Handbook*; Oh, C. H., Ed.; CRC Press: Boca Raton, FL, 2001.

(3) Anthony, E. J.; Wang, J. S. Pilot plant investigations of thermal remediation of tar-contaminated soil and oil-contaminated gravel. *Fuel* **2006**, *85*, 443−450.

(4) Vidonish, J. E.; Zygourakis, K.; Masiello, C. A.; Sabadell, G.; Alvarez, P. J. Thermal Treatment of Hydrocarbon-Impacted Soils: A Review of Technology Innovation for Sustainable Remediation. *Engineering* **2016**, *2*, 426−437.

(5) O'Brien, P. L.; DeSutter, T. M.; Casey, F. X. M.; Khan, E.; Wick, A. F. Thermal remediation alters soil properties—a review. *J. Environ. Manage.* **2018**, *206*, 826−835.

(6) Rogers, J. A.; Tedaldi, D. J.; Kavanaugh, M. C.; Screening, A. Protocol for Bioremediation of Contaminated Soil. *Environ. Prog.* **1993**, *12*, 146−156.

(7) Hinchee, R. E.; Semprini, L.; Ong, S. K. *Bioremediation of Chlorinated and Polycyclic Aromatic Hydrocarbon Compounds*; Lewis Publishers: Boca Raton, FL, 1994; p 525.

(8) Hinchee, R. E.; Kittel, J. A.; Reisinger, H. J. *Applied Bioremediation of Petroleum Hydrocarbons*; Battelle Press: Columbus, 1995; p 534.

(9) Stocking, A. J.; Deeb, R. A.; Flores, A. E.; Stringfellow, W.; Talley, J.; Brownell, R.; Kavanaugh, M. C. Bioremediation of MTBE: a review from a practical perspective. *Biodegradation* **2000**, *11*, 187−201.

(10) Soares, A. A.; Albergaria, J. T.; Domingues, V. F.; Alvim-Ferraz, M. D. M.; Delerue-Matos, C. Remediation of soils combining soil vapor extraction and bioremediation: Benzene. *Chemosphere* **2010**, *80*, 823−828.

(11) Zhang, Z. N.; Zhou, Q. X.; Peng, S. W.; Cai, Z. Remediation of petroleum contaminated soils by joint action of Pharbitis nil L. and its microbial community. *Sci. Total Environ.* **2010**, *408*, 5600−5605.
(12) Chibwe, L.; Geier, M. C.; Nakamura, J.; Tanguay, R. L.; Aitken, M. D.; Simonich, S. L. M. Aerobic Bioremediation of PAH Contaminated Soil Results in Increased Genotoxicity and Developmental Toxicity. *Environ. Sci. Technol.* **2015**, *49*, 13889−13898.
(13) Vidonish, J. E.; Zygourakis, K.; Masiello, C. A.; Gao, X.; Mathieu, J.; Alvarez, P. J. Pyrolytic treatment and fertility enhancement of soils contaminated with heavy hydrocarbons. *Environ. Sci. Technol.* **2016**, *50*, 2498−2506.
(14) Song, W.; Vidonish, J. E.; Kamath, R.; Yu, P. F.; Chu, C.; Moorthy, B.; Gao, B. Y.; Zygourakis, K.; Alvarez, P. J. J. Pilot-Scale Pyrolytic Remediation of Crude-Oil-Contaminated Soil in a Continuously-Fed Reactor: Treatment Intensity Trade-Offs. *Environ. Sci. Technol.* **2019**, *53*, 2045−2053.
(15) Vidonish, J. E.; Alvarez, P. J. J.; Zygourakis, K. Pyrolytic Remediation of Oil-Contaminated Soils: Reaction Mechanisms, Soil Changes, and Implications for Treated Soil Fertility. *Ind. Eng. Chem. Res.* **2018**, *57*, 3489−3500.
(16) Li, D. C.; Xu, W. F.; Mu, Y.; Yu, H. Q.; Jiang, H.; Crittenden, J. C. Remediation of Petroleum-Contaminated Soil and Simultaneous Recovery of Oil by Fast Pyrolysis. *Environ. Sci. Technol.* **2018**, *52*, 5330−5338.
(17) Kang, C. U.; Kim, D. H.; Khan, M. A.; Kumar, R.; Ji, S. E.; Choi, K. W.; Paeng, K. J.; Park, S.; Jeon, B. H. Pyrolytic remediation of crude oil-contaminated soil. *Sci Total Environ.* **2020**, 713−720.
(18) Riser-Roberts, E. *Remediation of Petroleum Contaminated Soils: Biological, Physical, and Chemical Processes*; CRC Press: Boca Raton, FL, 1998.
(19) Khan, F. I.; Husain, T.; Hejazi, R. An overview and analysis of site remediation technologies. *J. Environ. Manage.* **2004**, *71*, 95−122.
(20) Savage, P. E.; Klein, M. T.; Kukes, S. G. Asphaltene reaction pathways. 1. Thermolysis. *Ind. Eng. Chem. Proc. Des. Dev.* **1985**, *24*, 1169−1174.
(21) Banerjee, D. K.; Laidler, K. J.; Nandi, B. N.; Patmore, D. J. Kinetic studies of coke formation in hydrocarbon fractions of heavy crudes. *Fuel* **1986**, *65*, 480−484.
(22) LaMarca, C.; Libanati, C.; Klein, M. T.; Cronauer, D. C. Enhancing chain transfer during coal liquefaction: A model system analysis. *Energy Fuels* **1993**, *7*, 473−478.
(23) Savage, P. E. Mechanisms and kinetics models for hydrocarbon pyrolysis. *J. Anal. Appl. Pyrolysis* **2000**, *54*, 109−126.
(24) Yasar, M.; Trauth, D. M.; Klein, M. T. Asphaltene and resid pyrolysis. 2. The effect of reaction environment on pathways and selectivities. *Energy Fuels* **2001**, *15*, 504−509.
(25) Gray, M. R.; McCaffrey, W. C. Role of chain reactions and olefin formation in cracking, hydroconversion, and coking of petroleum and bitumen fractions. *Energy Fuels* **2002**, *16*, 756−766.
(26) Wauters, S.; Marin, G. B. Kinetic modeling of coke formation during steam cracking. *Ind. Eng. Chem. Res.* **2002**, *41*, 2379−2391.
(27) Van Speybroeck, V.; Van Neck, D.; Waroquier, M.; Wauters, S.; Saeys, M.; Marin, G. B. Ab initio study on elementary radical reactions in coke formation. *Int. J. Quantum Chem.* **2003**, *91*, 384−388.
(28) Van Speybroeck, V.; Hemelsoet, K.; Minner, B.; Marin, G. B.; Waroquier, M. Modeling elementary reactions in coke formation from first principles. *Mol. Simul.* **2007**, *33*, 879−887.
(29) Gao, Y.; Zygourakis, K. Kinetic Study of the Pyrolytic Treatment of Petroleum Contaminated Soils. *Ind. Eng. Chem. Res.* **2019**, *58*, 10829−10843.
(30) Vand, V. A theory of the irreversible electrical resistance changes of metallic films evaporated in vacuum. *Proc. Phys. Soc.* **1943**, *55*, 0222−0246.
(31) Pitt, G. J. The Kinetics of the Evolution of Volatile Products from Coal. *Fuel* **1962**, *41*, 267−274.
(32) Anthony, D. B.; Howard, J. B. Coal Devolatilization and Hydrogasification. *AIChE J.* **1976**, *22*, 625−656.
(33) Aboyade, A. O.; Carrier, M.; Meyer, E. L.; Knoetze, J. H.; Gorgens, J. F. Model fitting kinetic analysis and characterisation of the devolatilization of coal blends with corn and sugarcane residues. *Thermochim. Acta* **2012**, *530*, 95−106.
(34) de Caprariis, B.; Filippis, De.; Herce, P.; Verdone, C.; Double-Gaussian, N. Distributed Activation Energy Model for Coal Devolatilization. *Energy Fuels* **2012**, *26*, 6153−6159.
(35) Cai, J. M.; Liu, R. H. New distributed activation energy model: Numerical solution and application to pyrolysis kinetics of some types of biomass. *Bioresour. Technol.* **2008**, *99*, 2795−2799.
(36) Mani, T.; Murugan, P.; Mahinpey, N. Determination of Distributed Activation Energy Model Kinetic Parameters Using Simulated Annealing Optimization Method for Nonisothermal Pyrolysis of Lignin. *Ind. Eng. Chem. Res.* **2009**, *48*, 1464−1467.
(37) Cai, J. M.; Jin, C. A.; Yang, S. Y.; Chen, Y. Logistic distributed activation energy model—Part 1: Derivation and numerical parametric study. *Bioresour. Technol.* **2011**, *102*, 1556−1561.
(38) Cai, J. M.; Yang, S. Y.; Li, T. Logistic distributed activation energy model—Part 2: Application to cellulose pyrolysis. *Bioresour. Technol.* **2011**, *102*, 3642−3644.
(39) Cai, J. M.; Wu, W. X.; Liu, R. H.; Huber, G. W. A distributed activation energy model for the pyrolysis of lignocellulosic biomass. *Green Chem.* **2013**, *15*, 1331−1340.
(40) Cai, J. M.; Wu, W. X.; Liu, R. H. An overview of distributed activation energy model and its application in the pyrolysis of lignocellulosic biomass. *Renewable Sustainable Energy Rev.* **2014**, *36*, 236−246.
(41) Zhang, J. Z.; Chen, T. J.; Wua, J. L.; Wu, J. H. A novel Gaussian-DAEM-reaction model for the pyrolysis of cellulose, hemicellulose and lignin. *RSC Adv.* **2014**, *4*, 17513−17520.
(42) Skipper, N. T.; Soper, A. K.; Mcconnell, J. D. C. The Structure of Interlayer Water in Vermiculite. *J. Chem. Phys.* **1991**, *94*, 5751−5760.
(43) Fajnor, V. S.; Jesenak, K. Differential thermal analysis of montmorillonite. *J. Therm. Anal.* **1996**, *46*, 489−493.
(44) Sposito, G.; Skipper, N. T.; Sutton, R.; Park, S. H.; Soper, A. K.; Greathouse, J. A. Surface geochemistry of the clay minerals. *Proc. Natl. Acad. Sci. U.S.A.* **1999**, *96*, 3358−3364.
(45) Hensen, E. J. M.; Smit, B. Why clays swell. *J. Phys. Chem. B* **2002**, *106*, 12664−12667.
(46) Stackhouse, S.; Coveney, P. V.; Benoit, D. M. Density-functional-theory-based study of the dehydroxylation behavior of aluminous dioctahedral 2: 1 layer-type clay minerals. *J. Phys. Chem. B* **2004**, *108*, 9685−9694.
(47) Dolinar, B.; Macuh, B. Determining the thickness of adsorbed water layers on the external surfaces of clay minerals based on the engineering properties of soils. *Appl. Clay Sci.* **2016**, *123*, 279−284.
(48) Skipper, N. T.; Refson, K.; Mcconnell, J. D. C. Computer-Simulation of Interlayer Water in 2-1 Clays. *J. Chem. Phys.* **1991**, *94*, 7434−7445.
(49) Bray, H. J.; Redfern, S. A. T. Kinetics of dehydration of Ca-montmorillonite. *Phys. Chem. Miner.* **1999**, *26*, 591−600.
(50) Hupers, A.; Kopf, A. J. Effect of smectite dehydration on pore water geochemistry in the shallow subduction zone: An experimental approach. *Geochem. Geophys. Geosyst.* **2012**, *13*, No. 004212.
(51) Levy, J. H. Effect of Water-Vapor Pressure on the Dehydration and Dehydroxylation of Kaolinite and Smectite Isolated from Australian Tertiary Oil Shales. *Energy Fuels* **1990**, *4*, 146−151.
(52) Frost, R. L.; Vassallo, A. M. The dehydroxylation of the kaolinite clay minerals using infrared emission spectroscopy. *Clays Clay Miner.* **1996**, *44*, 635−651.
(53) Frost, R. L.; Ruan, H.; Kloprogge, J. T.; Gates, W. P. Dehydration and dehydroxylation of nontronites and ferruginous smectite. *Thermochim. Acta* **2000**, *346*, 63−72.
(54) Plante, A. F.; Fernández, J. M.; Leifeld, J. Application of thermal analysis techniques in soil science. *Geoderma* **2009**, *153*, 1−10.
(55) Brewer, C. E.; Hall, E. T.; Schmidt-Rohr, K.; Laird, D. A.; Brown, R. C.; Zygourakis, K. Temperature and reaction atmosphere effects on the properties of corn stover biochar. *Environ. Prog. Sustainable Energy* **2017**, *36*, 696−707.

https://doi.org/10.1021/acs.est.1c03607
Environ. Sci. Technol. 2021, 55, 11987−11996

(56) Killingley, J. S.; Day, S. J. Dehydroxylation Kinetics of Kaolinite and Montmorillonite from Queensland Tertiary Oil-Shale Deposits. *Fuel* **1990**, *69*, 1145−1149.
(57) Patterson, J. H.; Hurst, H. J.; Levy, J. H.; Killingley, J. S. Mineral Reactions in the Processing of Australian Tertiary Oil Shales. *Fuel* **1990**, *69*, 1119−1123.
(58) Shin, S.; Im, S. I.; Kwon, E. H.; Na, J.-G.; Nho, N. S.; Lee, K. B. Kinetic study on the nonisothermal pyrolysis of oil sand bitumen and its maltene and asphaltene fractions. *J. Anal. Appl. Pyrolysis* **2017**, *124*, 658−665.
(59) Ranjbar, M. Influence of reservoir rock composition on crude oil pyrolysis and combustion. *J. Anal. Appl. Pyrolysis* **1993**, *27*, 87−95.
(60) Verkoczy, B. Factors affecting coking in heavy oil cores, oils and SARA fractions under thermal stress. *J. Can. Pet. Technol.* **1993**, *32*, 25−33.
(61) Radmanesh, R.; Chan, E.; Gray, M. R. Modeling of mass transfer and thermal cracking during the coking of Athabasca residues. *Chem. Eng. Sci.* **2008**, *63*, 1683−1691.
(62) Kramers, H.; Alberda, G. Frequency Response Analysis of Continuous Flow Systems. *Chem. Eng. Sci.* **1953**, *2*, 173−181.
(63) Deans, H. A.; Lapidus, L. A Computational Model for Predicting and Correlating the Behavior of Fixed-Bed Reactors. 1. Derivation of Model for Nonreactive Systems. *AIChE J.* **1960**, *6*, 656−663.
(64) Deans, H. A.; Lapidus, L. A Computational Model for Predicting and Correlating the Behavior of Fixed-Bed Reactors. 2. Extension to Chemically Reactive Systems. *AIChE J.* **1960**, *6*, 663−668.
(65) Sinkule, J.; Hlavacek, V.; Votruba, J.; Tvrdik, I. Modeling of Chemical Reactors. 29. Mixing-Cell Model for Packed-Bed Reactors—Steady-State Considerations Problems of Multiplicity. *Chem. Eng. Sci.* **1974**, *29*, 689−696.
(66) Saterbak, A.; Toy, R. J.; Wong, D. C. L.; McMain, B. J.; Williams, M. P.; Dorn, P. B.; Brzuzy, L. P.; Chai, E. Y.; Salanitro, J. P. Ecotoxicological and analytical assessment of hydrocarbon-contaminated soils and application to ecological risk assessment. *Environ. Toxicol. Chem.* **1999**, *18*, 1591−1607.
(67) Kwon, M. J.; Hwang, Y. Assessing the Potential of Organic Solvents on Total Petroleum Hydrocarbon Extraction from Diesel-Contaminated Soils. *Water, Air, Soil Pollut.* **2017**, *228*, No. 189.
(68) Rawlings, J. B.; Ekerdt, J. G. *Chemical Reactor Analysis and Design Fundamentals*, 2nd ed.; Nob Hill Publishing: LLC: Santa Barbara, 2020; pp 144−162.
(69) Abatzoglou, N.; Chornet, E.; Belkacemi, K.; Overend, R. P. Phenomenological Kinetics of Complex-Systems—the Development of a Generalized Severity Parameter and Its Application to Lignocellulosics Fractionation. *Chem. Eng. Sci.* **1992**, *47*, 1109−1122.
(70) Antal, M. J.; Varhegyi, G.; Jakab, E. Cellulose pyrolysis kinetics: Revisited. *Ind. Eng. Chem. Res.* **1998**, *37*, 1267−1275.

https://doi.org/10.1021/acs.est.1c03607
Environ. Sci. Technol. 2021, 55, 11987−11996